Microstructure evolution of laser solid forming of Ti-Al-V ternary system alloys from blended elemental powders

Hua Tan (谭 华)[1], Fengying Zhang (张凤英)[1,2], Jing Chen (陈 静)[1], Xin Lin (林 鑫)[1], and Weidong Huang (黄卫东)[1*]

[1]*State Key Laboratory of Solidification Processing, Northwestern Polytechnical University, Xi'an 710072, China*

[2]*School of Materials Science and Engineering, Chang'an University, Xi'an 710064, China*

[*]*Corresponding author: huang@nwpu.edu.cn*

Received December 14, 2010; accepted January 28, 2011; posted online April 22, 2011

Morphology evolution of prior β grains of laser solid forming (LSF) Ti-xAl-yV ($x \leqslant 11$,$y \leqslant 20$) alloys from blended elemental powders is investigated. The formation mechanism of grain morphology is revealed by incorporating columnar to equiaxed transition (CET) mechanism during solidification. The morphology of prior β grains of LSF Ti-6Al-yV changes from columnar to equiaxed grains with increasing element V content from 4 to 20 wt.-%. This agrees well with CET theoretical prediction. Likewise, the grain morphology of LSF Ti-xAl-2V from blended elemental powders changes from large columnar to small equiaxed with increasing Al content from 2 to 11 wt.-%. The macro-morphologies of LSF Ti-8Al-2V and Ti-11Al-2V from blended elemental powders do not agree with CET predictions. This is caused by the increased disturbance effects of mixing enthalpy with increasing Al content, generated in the alloying process of Ti, Al, and V in the molten pool.

OCIS codes: 140.3590, 140.3390, 160.2120.

doi: 10.3788/COL201109.051403

Laser solid forming (LSF) has been recognized as a new additive in the manufacturing process that can build near-net-shape metallic components using the solid freeform fabrication route[1−3]. During LSF, powder is fed into a molten pool created by a laser beam. Parts are built in a point-by-point and layer-by-layer manner. LSF is particularly attractive for the manufacture of titanium aerospace components because it is expected to provide significant impact on the fabrication of components with intricate design complexity in the aerospace industry. Thus, a number of recent efforts have been conducted on LSF titanium alloys. This is especially true for Ti-6Al-4V, which has been widely used in the aerospace industry for its high strength-to-weight ratio. Crespo *et al*. developed a model combining finite element heat transfer calculations[4], phase transformation kinetics, and microstructure-property relations in Ti-6Al-4V. Processing maps relating the deposition parameters to the microstructure and properties of the parts were obtained using this model. Bontha *et al*. investigated the effects of process variables on grain morphologies of LSF Ti-6Al-4V[5]. Jia *et al*. developed a finite element model to simulate the temperature and stress field of LSF Ti-6Al-4V hollow blade[6]. However, previous studies showed that as-deposited Ti-6Al-4V alloy by LSF has higher strength and lower ductility compared with wrought Ti-6Al-4V[1,7]. Thus, Ti-6Al-4V may not be the optimum composition for LSF in Ti-Al-V ternary system alloys. In addition, LSF technology is expected to generate significant application in the repair of damaged expensive parts. Therefore, a key problem to be solved is how to realize performance matching during laser repair of Ti-6Al-4V forgings or castings. Investigating the microstructure and mechanical properties of LSF Ti-xAl-yV alloys is necessary. This will be helpful in developing a special Ti-xAl-yV alloy for LSF technology to improve the mechanical properties of LSF titanium alloy. Furthermore, this will lay a foundation for performance matching in laser repair of Ti-6Al-4V damaged parts. Performance matching can be realized by depositing a special Ti-xAl-yV alloy with mechanical properties close to the damaged parts.

Generally, pre-alloyed powders have been used as the deposited materials in LSF. However, since the powders are synchronously injected into the molten pool and pass through re-melting and re-solidification processes, it is convenient to deposit a blend of elemental powders and create an alloy *in situ* in LSF. This is a powerful tool in the investigation of new alloy systems and in the creation of innovative materials. In addition, LSF from blended elemental powders could potentially reduce processing costs to a large extent. A number of recent efforts have been conducted on LSF titanium alloys from blended elemental powders[8−12].

In the present study, Ti-xAl-yV ($x \leqslant 11$, $y \leqslant 20$) titanium alloys were deposited by LSF from blended elemental powders. The morphology evolution of prior β grains of LSF Ti-xAl-yV alloys was investigated. Furthermore, the formation mechanism of the grain morphology was demonstrated by incorporating the columnar to equiaxed transition (CET) mechanism during solidification and mixing enthalpy calculation for Ti, Al, and V.

The deposited materials used in the experiments included commercially pure Ti, Al, and V powders, whose characteristics are shown in Table 1. The powders were dried for over 24 h in a vacuum drying furnace with 110 °C and then mixed in a ball grinder for 2 h.

The Ti-xAl-yV ($x \leqslant 11$, $y \leqslant 20$) alloy samples were deposited using an LSF system that consisted of a 5-kW continuous wave CO_2 laser, four-axis numerical control working table, high precision powder feeder, and a coaxial nozzle with four symmetrical powder nozzle tips. The

experiments were conducted inside a glove box filled with argon gas. Schematic of the LSF system is presented in Fig. 1. The substrates were pure Ti sheets, and argon was employed as the carrier gas and the shielding gas. During the formation process, the laser beam was directed on the substrate to create a moving molten pool into which a mixture of blended elemental powders was injected through the nozzle. Thin wall samples of 50×12×3 (mm) were deposited. The processing parameters are presented in Table 2.

The compositions and microstructures of as-deposited samples were characterized by an inductively coupled plasma atomic emission spectrometer (ICP-AES) and through optical microscopy (OM), respectively.

Figures 2(a)−(e) show the typical optical macromorphologies of Ti-6Al-4V, Ti-6Al-10V, and Ti-6Al-20V alloys deposited from blended elemental powders under the same processing conditions. Deposits of Ti-6Al-4V and Ti-6Al-10V are dominated by large columnar grains (with an average grain width of 300−1000 μm). The growth direction is essentially perpendicular to the substrate, and some smaller sizes of equiaxed grains exist at the very top. With an increase of V content from 10 to 20 wt.-%, the prior β grains change from epitaxial large columnar grains to small equiaxed grains, as shown clearly in Figs. 2(b) and (c). The prior β grains in the deposits of Ti-6Al-20V noticeably exhibit a more elongated morphology at the bottom and middle than that at the topmost part. The width of the grains is approximately

Table 1. Characteristics of the Deposited Materials

Powder Material	Equivalent Particle Diameter (μm)	Oxygen Content (wt.%)
Ti	131.40	0.069
Al	83.55	0.090
V	56.81	0.071

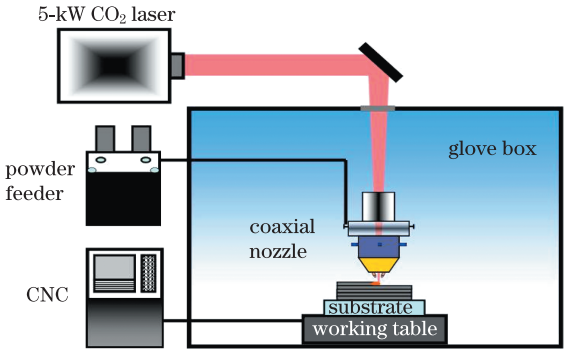

Fig. 1. Schematic of the LSF system.

Table 2. Processing Parameters of the LSF Route

Laser Power (W)	Scanning Velocity (mm/s)	Spot Diameter (mm)
1800−2300	5	3.0
Powder Feeding Rate (g/s)		Carrier Gas Flow (m^3/s)
7.5×10^{-2}		5×10^{-5}

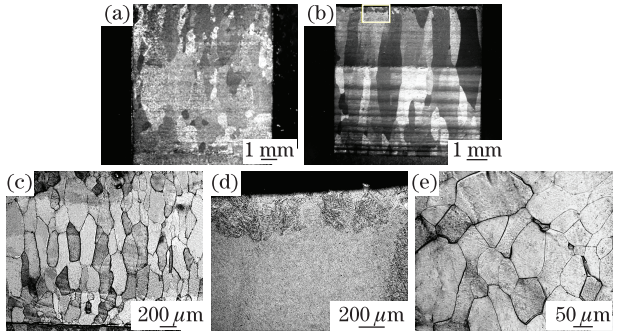

Fig. 2. Morphologies of LSF Ti-6Al-yV alloys from blended elemental powders: (a) Ti-6Al-4V; (b) Ti-6Al-10V; (c) bottom of Ti-6Al-20V; (d) highly magmified image OM image ofthe top of Ti-6Al-10V; (e) top of Ti-6A1-20V.

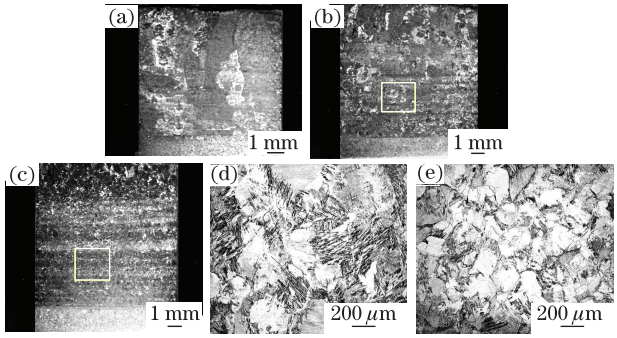

Fig. 3. Morphologies of LSF Ti-xAl-2V alloys from blended elemental powders: (a) Ti-4Al-2V; (b) Ti-8Al-2V; (c) Ti-11Al-2V; (d) highly magnified OM image of Ti-8Al-2V; (e) highly magnified OM image of Ti-11Al-2V.

100−200 μm and the length is within 200−500 μm at the bottom and middle. The grain width and length are approximately 50–100 μm at the topmost part of the deposits. Figures 2(d) and (e) show that the size of the equiaxed grains at the topmost part of Ti-6Al-20V is considerably smaller than that of Ti-6Al-10V. Thus, CET tends to occur with the increase of element V content in LSF Ti-6Al-yV alloys.

Figures 3(a)−(e) show the grain morphologies of LSF Ti-2Al-2V, Ti-8Al-2V, and Ti-11Al-2V from blended elemental powders under the same processing parameters. With an increase of mass content of Al, the prior β grains in LSF Ti-xAl-2V change from epitaxial columnar grains to equiaxed grains, and the grain size gradually decreases from 700−2000 μm (width) and 1000−6000 μm (length) to 100−300 μm (length and width). In addition, the β grains at the topmost part of Ti-8Al-2V and Ti-11Al-2V laser deposits tend to grow epitaxially even though the deposits are dominated by equiaxed grains.

To understand the observed microstructure evolution, the conditions under which CET will occur for Ti-6Al-yV and Ti-xAl-2V were obtained using Lin's model[13]. The shaded rectangles in Figs. 4 and 5 represent the range of solidification conditions during LSF. The arrow paths in the figures show the progress of the solidification condition of the molten pool under the laser processing parameters. During solidification, the crystal growth velocity increases rapidly from zero at the bottom of the molten pool to a value close to the laser scanning velocity at the molten pool surface. The temperature gradient is highest at

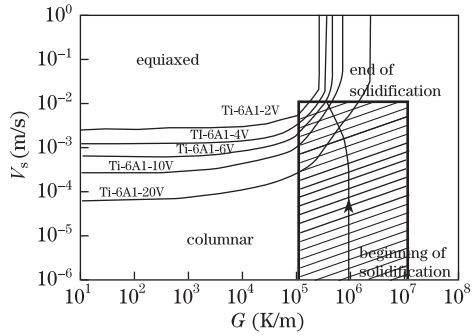

Fig. 4. CET curves for Ti-6Al-yV ($y \leqslant 20$) alloys showing regions of columnar dendrites and equiaxed dendrites as a function of solidification parameters G and V_s.

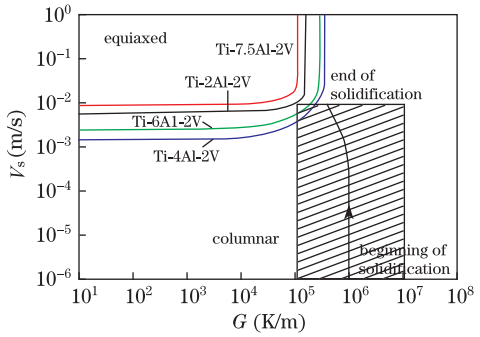

Fig. 5. CET curves for Ti-xAl-2V ($x \leqslant 11$) alloys showing regions of columnar dendrites and equiaxed dendrites as a function of solidification parameters G and V_s.

solidification initiation and decreases subsequently as the surface of the molten pool started to solidify. Under the present conditions, columnar crystal growth dominates the initial process in the solidification of each deposited layer, and the CET condition is attained at the end of the solidification. Theoretically, the tail of the molten pool is most vulnerable to the occurrence of CET. Figure 4 shows CET is not prone to occur in most regions when Ti-6Al-4V and Ti-6Al-10V samples are deposited. CET can occur only at the top of each layer because the temperature gradient G is lowest in this layer and the solidification velocity V_s is highest at the tail of the molten pool. When the next layer is deposited, the equiaxed grains at the top can be re-melted. Thus, β-Ti columnar grains will grow epitaxially along the deposit direction and the equiaxed grains are expected to form only at the top of the samples. However, for Ti-6Al-20V, CET will occur in more regions. Consequently, a large amount of equiaxed grains will be formed at the top region of each layer. When the next layer is deposited, several equiaxed grains at the top cannot be re-melted and the epitaxial growth of the columnar grains will be interrupted. Consequently, the equiaxed grains of elongated morphologies are formed. In addition, calculations in Fig. 4 suggest the probability of CET occurring with increasing V content in LSF Ti-6Al-yV ($y \leqslant 20$) at a certain condition. The experimental results shown in Fig. 2 agree well with theoretical predictions.

However, Fig. 5 shows that CET is not prone to occur in most regions containing laser deposits of Ti-2Al-2V, Ti-4Al-2V, Ti-6Al-2V, and Ti-7.5Al-2V. In addition, calculations show that Ti-8Al-2V and Ti-11Al-2V, which have an extremely small freezing range of ΔT_0 ($\Delta T_0 \approx 0$ K, Fig. 6), prevent CET occurrence under the positive temperature gradient condition. Thus, columnar crystal growth will dominate the LSF Ti-2Al-2V, Ti-8Al-2V, and Ti-11Al-2V microstructures. However, experimental results for Ti-8Al-2V and Ti-11Al-2V are different from theoretical predictions. Since few unmelted particles were found in the microstructures of the deposits, the mixing enthalpy of the constituent elements in the molten pool possibly played a crucial role. Using Miedema's theory[14] the mixing enthalpies ΔH_{mix} of Ti-xAl and Ti-yV alloys were calculated, the results of which are shown in Fig. 7. Clearly, the mixing of Ti-xAl and Ti-yV in the molten pool are exothermic processes and the liberated heat of Ti-xAl is considerably larger than that of Ti-yV. The crystal growth direction is known to be affected severely by the heat flow direction. The rapid increase of liberated heat of Ti-xAl-2V which resulted from increasing Al content may facilitate the change of heat flow direction in the local area ahead of the solid/liquid interface. Thus, when the next layer is deposited, the disturbance in heat flow may interrupt the epitaxial growth of the columnar grains along the deposit direction, and promote nucleation and growth of new grains ahead of the solid/liquid interface. This results in the formation of irregularly equiaxed grains. To eliminate the disturbance effect of the mixing enthalpy, a laser re-melting process was carried out on each deposited layer where the mixing enthalpy can be neglected in the re-melting process since the mixing process of the elements has been completed in the formation of the deposited layer. The obtained optical macro-morphology of Ti-11Al-2V is shown in Fig. 8. The large columnar grains dominate the entire deposit of Ti-11Al-2V, which agrees well with

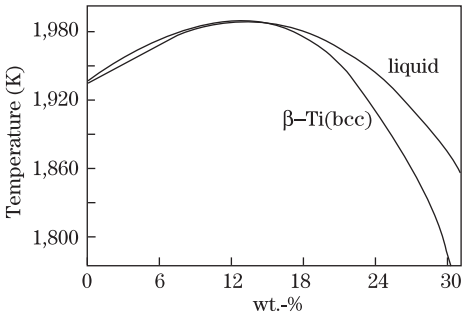

Fig. 6. Ti-xAl phase diagram in the concentration zone of Ti.

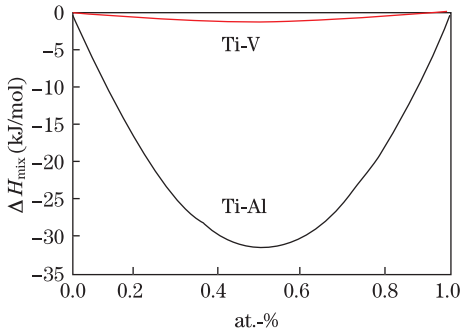

Fig. 7. Mixing enthalpies of Ti-Al and Ti-V.

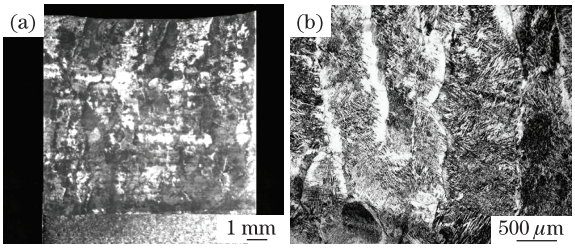

Fig. 8. Morphology of LSF Ti-11Al-2V alloy: (a) macrograph; (b) highly magnified OM image.

the CET prediction.

The microstructures of other LSF Ti-xAl-yV including Ti-4Al-yV, Ti-8Al-yV, Ti-xAl-4V, Ti-xAl-6V, and Ti-xAl-8V ($x \leqslant 11$, $y \leqslant 20$) were investigated as well. Results agree well with CET predictions.

In conclusion, the morphology evolution of prior β grains of LSF Ti-xAl-yV ($x \leqslant 11$, $y \leqslant 20$) alloys from blended elemental powders has been investigated. The formation mechanism of the grain morphology is revealed by combining the CET calculation during solidification and considering the disturbance effects of the mixing enthalpy of Ti, Al, and V elements in the molten pool. The grain morphologies of Ti-xAl-yV ($x \leqslant 11$, $y \leqslant 20$) are found in good agreement with CET calculations after eliminating the disturbance effect of the mixing enthalpy.

This work was supported by the State Key Laboratory of Solidification Processing in NWPU (Nos. SKLSP201102 and 06-BZ-2010)L, the China Postdoctoral Science Foundation (No.20100470040), and the National Natural Science Foundation of China (No. 50871089).

References

1. W. D. Huang, X. Lin, J. Chen, Z. X. Liu, and Y. M. Li, *Laser Solid Forming Technology* (in Chinese) (Northwestern Polytechnical University Press, Shaanxi, 2007).
2. X. Chen and X. Yang, Chinese J. Lasers (in Chinese) **37,** 842 (2010).
3. J. Wang, J. Chen, Y. Liu, X. Zhao, F. Ying, and W. Huang, Chinese J. Lasers (in Chinese) **37,** 847 (2010).
4. A. Crespo and R. Vilar, Scr. Mater. **63,** 140 (2010).
5. S. Bontha, N. W. Klingbeil, P. A. Kobryn, and H. L. Fraser, J. Mater. Process. Technol. **178,** 135 (2006).
6. W. Jia, X. Lin, J. Chen, H. Yang, C. Zhong, and W. Huang, Chinese J. Lasers (in Chinese) **34,** 1308 (2007).
7. S. Zhang, X. Lin, J. Chen, and W. Huang, Chin. Opt. Lett. **7,** 498 (2009).
8. R. Banerjee, D. Bhattacharyya, P. C. Collins, G. B. Viswanathan, and H. L. Fraser, Acta Mater. **52,** 377 (2004).
9. R. Banerjee, S. Nag, and H. L. Fraser, Mater. Sci. Eng. C **25,** 282 (2005).
10. S. Nag, R. Banerjee, and H. L. Fraser, Acta Biomater. **3,** 369 (2007).
11. R. Banerjee, A. Genc, D. Hill, P. C. Collins, and H. L. Fraser, Scr. Mater. **53,** 1433 (2005).
12. F. Zhang, J. Chen, H. Tan, X. Lin, and W. Huang, Chin. Opt. Lett. **7,** 222 (2009).
13. X. Lin, Y. M. Li, L. P. Feng, J. Chen, and W. D. Huang, Sci. China, Ser. E **33,** 476 (2003).
14. B. W. Zhang, *Theory of Embedded Atom Method and its Application to Materials Science*: *Atomic Scale Materials Design Theory* (in Chinese) (Hunan University Press, Changsha, 2003).